

1 **Effects of lateral processes on the seasonal water stratification of the**  
2 **Gulf of Finland: 3-D NEMO-based model study**

3

4 **R.E. Vankevich<sup>1,2</sup>, E.V. Sofina<sup>1,2</sup>, T.E. Eremina<sup>1</sup>, A.V. Ryabchenko<sup>2</sup>, M.S. Molchanov<sup>1</sup>,**  
5 **A.V. Isaev<sup>1,2</sup>**

6 [1]{Russian State Hydrometeorological University, Saint-Petersburg, Russia}

7 [2]{The St.-Petersburg Branch of the P.P.Shirshov Institute of Oceanology of the Russian  
8 Academy of Sciences}

9

10 Correspondence to: R.E. Vankevich (rvankevich@mail.ru)

11

12 **Abstract**

13 This paper is aimed to fill the gaps in knowledge of processes affecting the  
14 seasonal water stratification in the Gulf of Finland (GOF). We used state-of-the-art  
15 modeling framework NEMO designed for oceanographic research, operational  
16 oceanography, seasonal forecasting and climate studies to build an eddy resolving model  
17 of the GOF. To evaluate the model skill and performance two different solutions were  
18 obtained on 0.5 km eddy resolving and commonly used 2 km grids for one year simulation.  
19 We also explore the efficacy of nonhydrostatic effect (convection) parameterizations  
20 available in NEMO for coastal application. It is found that the solutions resolving sub-  
21 mesoscales have a more complex mixed layer structure in the regions of GOF directly  
22 affected by the upwelling/downwelling and intrusions from the open Baltic Sea. Presented  
23 model estimations of the upper mixed layer depth are in a good agreement with in situ  
24 CTD data. A number of model sensitivity tests to the vertical mixing parameterization  
25 confirm the model robustness. Further progress in the sub-mesoscale processes  
26 simulation and understanding is apparently connected mainly not with the finer resolution  
27 of the grids, but with the use of non-hydrostatic models because of the failure of  
28 hydrostatic approach at sub-mesoscale.

29

30 **Introduction**

31 The Gulf of Finland (GOF) is a 400 km long and 48–135 km wide sub-basin of the  
32 Baltic Sea with a mean depth of 37 m and complex bathymetry (see Fig. 1). The large  
33 fresh water input from Neva River significantly affects the stratification and forms the

34 strong salinity gradient from east to west and from north to south. Sea-surface salinity  
35 decreases from 5‰ to 6.5‰ in the western GOF to about 0‰–3‰ in the easternmost part  
36 of the Gulf where the role of the Neva River is most pronounced (Alenius et al., 1998). In  
37 the western GOF, a quasi-permanent halocline is located at a depth of 60–80 m. Salinity in  
38 that area can reach values as high as 8‰–10‰ near the sea bed due to the advection of  
39 saltier water masses from the Baltic Proper.

40 The vertical stratification in the GOF as well as in the Baltic Sea is unusual (the  
41 thermocline and halocline are usually separated) with a pronounced and relatively stable  
42 halocline, whereas the temperature is largely controlled by the seasonal variability of the  
43 surface heat fluxes (see e.g. Hankimo, 1964). During the summer season the water  
44 column in the deeper areas of the GOF consists of three layers – the upper mixed layer  
45 (UML), the cold intermediate layer and a saltier and slightly warmer near-bottom layer (see  
46 Liblik and Lips, 2012), separated by two pycnoclines – the thermocline at the depths of  
47 10–20 m and the permanent halocline at the depths of 60–70 m. A seasonal thermocline  
48 starts to develop in May. The surface mixed layer reaches a maximum depth of 15–20 m  
49 by midsummer and an erosion of the thermocline starts in late August due to wind mixing  
50 and thermal convection. The bottom salinity also shows significant spatiotemporal  
51 variability due to irregular saline water intrusions from the Baltic Proper, as well as from  
52 changes in river runoff and the precipitation-evaporation balance. There is no permanent  
53 halocline in the eastern GOF, where salinity increases approximately linearly with depth  
54 (Nekrasov and Lebedeva, 2002; Alenius et al., 2003).

55 The simulations of the vertical stratification using 3-D numerical models are not so  
56 reliable yet (Myrberg et al., 2010). This study shows that the most advanced 3-D  
57 circulation models are able to simulate the major features of the hydro-physical fields of  
58 the GOF. For example, generally the hind-cast temperatures differ from observations by  
59 less than 1–2°C and the mean error in salinity is less than 1‰. Most of the remaining  
60 difficulties are connected with problems in adequately representing the dynamics of the  
61 mixed layer. The loss of accuracy is most notable in the simulation of the depth and the  
62 sharpness of the corresponding thermo- and haloclines. Despite the application of  
63 sophisticated turbulent closure schemes and different schemes for vertical mixing, none of  
64 the models, analyzed in (Myrberg et al., 2010), were able to accurately simulate the  
65 vertical profiles of temperature and salinity. Latest experiments with turbulence  
66 parameterizations of 3-D hydrodynamic model COHERENS presented in (Tuomi et al.,  
67 2013) show that model still underestimates the thermocline depth. Also the sensitivity of  
68 the modelled thermocline depth to the accuracy of the meteorological forcing was studied

69 by increasing the forcing wind speed to better match the measured values of wind speed  
70 in the central GOF. The sensitivity test showed that an increase in the wind speed only  
71 slightly improved the performance of the turbulence parameterizations in modelling the  
72 thermocline depth.

73 However, a number of studies have reported important effects of the vertical  
74 thermohaline structure on the characteristics and processes in the marine ecosystems of  
75 the GOF, such as phytoplankton species composition (Rantajarvi et al., 1998) and sub-  
76 surface maxima of phytoplankton biomass (Lips et al., 2010), cyanobacteria blooms (Lips  
77 et al., 2008), distribution of pelagic fish (Stepputtis et al., 2011), macrozoobenthos  
78 abundance (Laine et al., 2007) and oxygen concentrations in the near bottom layer  
79 (Maximov, 2006).

80 Summarizing all written above, prediction of the thermohaline structure is a complex  
81 problem for the GOF. The spatial variability of the thermohaline structure encompasses a  
82 wide range of physical processes at different scales, some of which are still poorly  
83 understood (Soomere et al., 2008, 2009). For example, we hypothesize that the local  
84 stratification depends very strongly on the across GOF movements of water masses and  
85 that sub-mesoscale eddies generated by baroclinic instability of fronts in upper layers of  
86 the sea play an important role in heterogeneity of spatial distribution of parameters  
87 (temperature, nutrients, phytoplankton) but also they can contribute to re-stratify the UML,  
88 as described in Gent and McWilliams (1990).

89 In the ocean, submesoscales are scales of motion equal or less than the Rossby  
90 radius of deformation but large enough to be influenced by planetary rotation (Thomas et  
91 al., 2007). Recent studies showed that increasing the horizontal resolution of the model up  
92 to 0.5 km (for the GOF Rossby radius approx. 2–4 km) enables models to resolve  
93 submesoscale eddies. As a result, surface currents and temperatures show highly detailed  
94 patterns that qualitatively match well with the expected features ( Zhurbas et al., 2008;  
95 Sokolov, 2013) However, there was no yet considered the influence of eddy motions and  
96 across Gulf movements of water masses on vertical re-stratification of the UML of the  
97 GOF.

98 The motivations behind this study are:

- 99 – to provide an insight into the lateral advection processes in the GOF. We are  
100 interested, in particular, in estimating the contribution [of](#) lateral advection processes  
101 to the thermocline variations.
- 102 – to assess the impact of horizontal grid resolution on the representation of  
103 vertical stratification

104

105

## **Approach**

106

107

108

109

110

111

112

113

114

115

116

117

118

### **2.1 General Model set-up**

119

120

121

122

123

124

125

126

127

128

129

130

131

132

133

134

135

136

137

138

The traditional point of view is that the eddy diffusion dominates in the horizontal direction and in the vertical direction mixing due to eddies is limited, and small scale processes such as turbulence provide the majority of mixing. Based on this idea most commonly 1-D approach is used to set up vertical mixing by tuning a turbulent scheme. For the GOF as an enclosed basin with complex bathymetry and strong stratification mixed layer dynamics can be strongly affected by lateral advective processes. To investigate this phenomenon we present a state-of-the art three-dimensional model of the GOF with high vertical and two different horizontal resolutions. Shelf sea modelling is characterized by a demand for many different configurations to meet multiple science and user needs. NEMO gives the capability to rapidly configure shelf sea models using appropriate high resolutions and parameterizations for the representation of coastal dynamics.

Our study is based on a 3-D thermo-hydrodynamic model build on the NEMO (Nucleus for European Modelling of the Ocean) code initially designed for the open ocean and adopted by our team for the GOF (NEMO GOF). The NEMO is a 3-D hydrostatic, baroclinic primitive equation model toolkit laid out horizontally on the Arakawa C-grid (Madec et al., 1998; Madec, 2012). The NEMO is developing in a framework of a community European institutes and benefit of the recent scientific and technical developments implemented in most ocean modeling platforms. The NEMO implementation for the GOF uses the TVD advection scheme in the horizontal direction, the piecewise parabolic method (PPM) in the vertical direction (Liu and Holt, 2010), the non-linear variable volume (VVL) scheme for the free surface. In the horizontal plane, the model uses the standard Jacobean formulation for the pressure gradient, the viscosity and diffusivity formulation with a constant coefficient for momentum and tracer diffusion. The horizontal viscosity and diffusivity operators are rotated to be aligned with the density iso-surfaces to accurately reproduce density flows.

There are NEMO setups for Baltic Sea recently published by Hordoir et al. (2013 and 2015). The GOF setup was developed in parallel to the Baltic Sea model and aimed to introduce resolution able to resolve the sub-mesoscale processes in horizontal direction and insure accurate representation of the vertical structure by increasing the vertical resolution to 1 m. General model setup for the GOF shares most of the parameterization and schemes with Baltic Sea model.

139 In this paper, we used gridded bathymetric data set with a resolution of 0.25 nm for  
140 the GOF (Andrejev, 2010). Choosing different grid resolutions of the model is formally  
141 equivalent to the choice of an appropriate averaging operator (low-pass filtering at the grid  
142 step) and an approach to estimate the contribution of smaller scales to the general motion.  
143 To assess the impact of submesoscale motion on the vertical stratification, two  
144 configurations of NEMO GOF were generated by utilizing different horizontal and the same  
145 vertical resolution of 1m. Both configurations have 94 vertical levels, but 1 minute zonal  
146 and 2 minute meridional resolution (~2km) in a standard configuration and 0.25 minute  
147 zonal and 0.5 minute meridional resolution (~0.5km) in a finer resolution configuration. The  
148 parameters of configurations were kept as identical as possible. The main exception is the  
149 coefficients of horizontal diffusivity and viscosity which were set to the minimum values  
150 guaranteeing the numerical stability.

151 Numerical experiments were started from rest and initialized with temperature and  
152 salinity fields from the operational model of Baltic Sea HIROMB (Funkquist, 2001). The  
153 computational domain covers the entire GOF with the open boundary set at 23E longitude  
154 (see Fig. 1), boundary conditions being taken also from HIROMB. According to the inter-  
155 comparison of several models results for GOF (Myrberg et al., 2010), HIROMB was rated  
156 as the best model for the western part of the GOF. The operational status of the model  
157 gave us additional benefit. The model was forced by the surface forcing dataset HIRLAM  
158 (<http://hirlam.org>) (using the CORE bulk forcing algorithm) and climatic rivers runoff  
159 (Stalnacke et al., 1999). We used SMHI version of HIROMB with HIRLAM atmospheric  
160 fields included in output files as a part of a standard operational product of SMHI.  
161 Temporal resolution for the atmospheric forcing and boundary conditions is 1 hour.

162

## 163 **2.2 Parameterization of convective flows**

164 One of the possible mechanisms by which the lateral motion affects the stratification  
165 is a shear-induced convection: situation in which heavy water may be advected on top of  
166 lighter water. This mechanism has been observed, e.g. in the bottom boundary layer of  
167 lakes (Lorke et al., 2005) and on the continental shelf (Rippeth et al., 2001). Evidently, the  
168 shear-induced convection can take place throughout the water column, for example,  
169 during upwelling. In nature, convective processes quickly re-establish the static stability of  
170 the water column (Umlauf, 2005). These processes have been removed from the model  
171 via the hydrostatic assumption so they must be parameterized.

172 Convective mixing can be parameterized in NEMO by : (1) a computationally  
173 efficient solution 'TKE (turbulent kinetic energy) scheme' in combination with convective

174 adjustment procedures (a non-penetrative convective adjustment or an enhanced vertical  
 175 diffusion) and (2) physically more accurate the "GLS (generic length scale) scheme".

176 The "TKE scheme" is a turbulence closure scheme proposed by Bougeault and  
 177 Lacarrère (1989) originally developed to a model for the atmospheric boundary layer. In  
 178 the Mellor and Yamada (1974) hierarchy it is a 1.5-level closure and consists of a  
 179 prognostic closure for the turbulent kinetic energy (TKE) and an algebraic formulation for  
 180 the mixing length scale. The time evolution of TKE is the result of the production of TKE  
 181 through vertical shear, its suppression through stratification, its vertical diffusion, and its  
 182 dissipation of Kolmogorov (1942) type:

$$183 \quad \frac{d\overline{k}}{dt} = \overline{P} - \overline{\epsilon} + \overline{\nabla \cdot (K_m \nabla k)}, \quad (1)$$

$$184 \quad \overline{\epsilon} = C_\epsilon \frac{\overline{k}^2}{l_\epsilon}, \quad (2)$$

$$185 \quad l_k = C_k \frac{\overline{k}}{N}, \quad (3)$$

186 where  $N$  is the local buoyancy frequency,  $l_\epsilon$  and  $l_k$  are the dissipation and mixing length  
 187 scales,  $u$  and  $v$  are the horizontal velocity components,  $k$  is the layer number,  $e_3 = 1$  m is  
 188 the vertical scale factor,  $Pr_t$  is the Prandtl number,  $K_m$  and  $K_\rho$  are the vertical eddy viscosity  
 189 and diffusivity coefficients. The parameter  $C_k$  is known as a stability function and is defined  
 190 as a constant in the TKE scheme. The constants  $C_k = 0.1$  and  $C_\epsilon = 0.7$  are specified to  
 191 deal with vertical mixing at any depth (Gaspar et al., 1990).  $K_e$  is the eddy diffusivity  
 192 coefficient for the TKE. In NEMO  $K_e = K_m$ .

193 For computational efficiency, the original formulation of the turbulent length scales  
 194 proposed by Gaspar et al. (1990) has been simplified to the following first order  
 195 approximation

$$196 \quad l_k = \frac{K_m}{\overline{u}'} \quad (4)$$

197 This simplification valid in a stable stratified region with constant values of the  
 198 buoyancy frequency has two major drawbacks: it makes no sense for locally unstable  
 199 stratification and the computation no longer uses all the information contained in the  
 200 vertical density profile. To overcome these drawbacks, NEMO TKE scheme  
 201 implementation adds an extra assumption concerning the vertical gradient of the computed  
 202 length scale. So, the length scales are first evaluated as in (4) and then bounded such  
 203 that:

$$204 \quad l_k \leq l_{up} \text{ and } l_k \leq l_{down}, \text{ with} \quad (5)$$

205 In order to impose the constraint (5), NEMO introduces two additional length scales:  
 206  $l_{up}$  and  $l_{down}$ . The length scales  $l_{up}$  and  $l_{down}$  are respectively the upward and downward  
 207 distances to which a fluid parcel is able to travel from current z-level  $k$ , converting its TKE

208 into the potential energy by doing work against the stratification, and they can be  
 209 evaluated as:  $\epsilon = \sum_{k=1}^{nk} \epsilon_k$

$$210 \quad \epsilon_k = \frac{1}{2} \rho \sum_{i,j} \overline{u_i u_j u_i u_j} \quad \text{from } k = 1 \text{ to } nk \quad (6)$$

$$211 \quad \epsilon_k = \frac{1}{2} \rho \sum_{i,j} \overline{u_i u_j u_i u_j} \quad \text{from } k = nk \text{ to } 1, \quad (7)$$

212 where  $nk$  is the number of level in vertical,  $f^{(k)}$  is computed using (4), i.e.

$$213 \quad f^{(k)} = \frac{1}{2} \rho \sum_{i,j} \overline{u_i u_j u_i u_j} \quad (8)$$

$$214 \quad \text{Finally, } \epsilon = \sum_{k=1}^{nk} \epsilon_k \quad (9)$$

216 The GLS scheme is formally equivalent to the TKE scheme, excepting using: (1) a  
 217 prognostic equation for the generic length scale  $l$  and (2) expressions for the complex  
 218 stability functions instead constants. We used  $\epsilon$  turbulent closure scheme (Rodi, 1987)  
 219 with  $l = C_{lim} \sqrt{\epsilon / N^2}$ , where  $C_{lim}$  is a constant depending on the choice of the stability function  
 220 (Galperin et al., 1988; Kantha and Clayson, 1994).

221 This prognostic length scale is valid for convective situations and arbitrarily  
 222 increases diffusivity to represent convection (Umlauf and Burchard, 2003; 2005):

$$223 \quad \epsilon = \frac{1}{2} \rho \sum_{i,j} \overline{u_i u_j u_i u_j} \quad (10)$$

$$224 \quad \sqrt{\epsilon} = \frac{1}{2} \rho \sum_{i,j} \overline{u_i u_j u_i u_j} \quad (11)$$

$$225 \quad \overline{u_i u_j u_i u_j} = \frac{1}{2} \rho \sum_{i,j} \overline{u_i u_j u_i u_j} \quad (12)$$

$$226 \quad \overline{u_i u_j u_i u_j} = \frac{1}{2} \rho \sum_{i,j} \overline{u_i u_j u_i u_j} \quad (13)$$

227 Here  $C_1, C_2, C_3, C_{lim}$  are constants for the  $\epsilon$  turbulent closure scheme. They are equal  
 228 1.44, 1.92, 1.0, 1.3 respectively.  $C_1$  and  $C_2$  are calculated from the stability function.

229 As known, the equation fails in stably stratified flows, and for this reason almost all  
 230 authors apply a clipping of the length scale as an ad hoc remedy. With this clipping, the  
 231 maximum permissible length scale is determined by

$$232 \quad l = C_{lim} \sqrt{\epsilon / N^2} \quad (14)$$

233 A value of  $C_{lim} = 0.53$  is often used (Galperin et al., 1988). Umlauf and Burchard  
 234 (2005) show that the value of the clipping factor is of crucial importance for the  
 235 entrainment depth predicted in stably stratified flows. Another value is 0.26, several  
 236 authors have suggested limiting the dissipative length-scale in the presence of stable  
 237 stratification even down to 0.07 (Holt and Umlauf, 2008).

238 In addition, convective mixing can be parameterized in NEMO by an enhancement  
239 to the eddy viscosity and diffusivity (ED), if for  $N_2 < 0$ ,  $K_m$  and  $K_p$  are locally set to the value  
240 of  $100 \text{ m}^2\text{s}^{-1}$ .

241 We performed comparative tests of listed above convection parameterizations to  
242 investigate their principal applicability for shear-induced convective situations.

243

### 244 **3. Numerical experiments**

245 The modeling period was chosen from 1st April to 31st August 2011 when  
246 pronounced thermocline occurs. The thermocline starts its formation in early May when the  
247 surface heating and turbulent mixing are dominant processes. Note that year 2011 was  
248 characterized by strong upwelling events in the beginning and in the end of modeling  
249 period.

250 In section 3.1 the GLS, TKE and ED mixing parameterizations are compared in a  
251 series of sensitivity experiments. The choice of closure scheme and the effects of varying  
252 Galperin limit were investigated against MODIS SST to get the best reproduction of SST  
253 pattern.

254 In section 3.2 we present results of the model runs compared with available CTD  
255 data to study the performance of the chosen parameterizations to represent the UML  
256 evolution. Also the ability of the model to correctly capture such features as fronts was  
257 tested against SST images for different resolutions in beginning of August 2011 when  
258 there were cloud free images.

259

#### 260 **3.1. Sensitivity to vertical mixing parameterizations**

261 In this section we study closure schemes and enhanced diffusion parameterization  
262 performance for convective situations caused by upwelling near the Estonian coast started  
263 on May 12<sup>th</sup>. Figure 2 shows a cross section of the GOF for the density field (black  
264 isolines) overlaid by the vertical eddy diffusivity coefficient (color filled).

265 | Fragment A of Fig. 2 illustrates the mechanism instability formation. It is a  
266 hypothetical solution obtained with constant eddy diffusivity coefficients set to the minimum  
267 possible for this case values of  $10^{-4}$   $10^{-5} \text{ m}^2\text{s}^{-1}$  and ED switched off. All south-north cross  
268 sections present the situation mainly formed by an upwelling event near the Estonian  
269 coast (left side of the cross-section). Due to the presence of permanent density gradient  
270 from Estonian to Finish coast and strong offshore current caused by upwelling, dense  
271 | waters originated from the Estonian side overlay ~~more~~ fresher lighter water in the  
272 downwelling area near the Finish coast.



273 Fragment B illustrates the performance of the ED procedure setting the eddy  
274 viscosity and diffusivity coefficients equal to  $100 \text{ m}^2\text{s}^{-1}$  in the areas of unstable  
275 stratification. According to this experiment, the maximum depth of convection penetration  
276 is equal to 10 m in the center of GOF and reaches up to 25 m near the Finish coast.

277 Fragment C illustrates the performance of solution with the TKE closure scheme  
278 including previously described modifications introduced in NEMO. As seen, the solution  
279 demonstrates high values of eddy diffusion coefficients in the areas of unstable  
280 stratification. The depth of the mixed layer is not limited by the convection penetration  
281 depth (see Fig. 2b) and formed as a result of a joint action of current velocity shear,  
282 buoyancy and TKE diffusion and dissipation (see Eq. (1)).

283 Fragment D shows the combined effect of cases B and C. As seen from  
284 comparison of Fig. 2d and Fig. 2c, the solution with modified TKE scheme captures most  
285 of the existing instabilities. ED (Fig. 2b) triggered only in some small areas in the center of  
286 the mixed layer and did not affect the actual mixing depth.

287 Fragments E and F present the performance of the solution with the GLS closure  
288 scheme with Galperin limit of 0.53 and 0.26, correspondently. A solution with GLS  
289 parameterization with switched-off length scale limitation was also obtained but turned out  
290 to be practically equal to the case E. UML depth in these solutions is comparable to that in  
291 the cases C and D confirming success of TKE modifications in NEMO.

292 The above tests confirm that both TKE and GLS closure schemes used in NEMO  
293 are able to catch the convection induced by upwelling. As it comes from Fig. 2 an  
294 instability of vertical column initiates dramatic increasing in vertical diffusivity coefficients  
295 up to  $0.04 \text{ m}^2\text{s}^{-1}$  TKE (Fig. 2c and d) or  $0.036 \text{ m}^2\text{s}^{-1}$  GLS (Fig. 2e and f) from the  
296 background value set to  $10^{-6} \text{ m}^2\text{s}^{-1}$ . TKE scheme forms a core with stronger mixing in the  
297 area of downwelling but at the same time the UML depth is comparable in both cases.  
298 Switched on ED does not modify the UML depth predicted by turbulent closure schemes.

299 Evaluation of the actual performance of presented alternative parameterizations of  
300 convective processes is a complex task requiring high spatial and temporal resolution of in  
301 situ data that is not available at the moment. The sea surface temperature (SST) derived  
302 from the satellite thermal infrared imagery during cloud-free conditions provides significant  
303 information for monitoring of the relevant key ocean structures, such as fronts, eddies, and  
304 upwelling. At the same time, the SST fields can be used as an indicator of vertical mixing  
305 processes. SST fields can be considered as integral of subsurface dynamic but for  
306 example we can not estimate directly a depth of the thermocline from them. Alternatively  
307 the comparison of the modeled frontal structure at the sea surface and MODIS data during

308 an upwelling event (lifting water from under the UML) could indicate how well the model  
309 reproduces stratification. As soon as we would get a realistic stratification, the surface  
310 pattern of simulated SST will also be in agreement with remotely observed SST.

311 Results of the comparison of modeled (various mixing parameterizations and  
312 resolutions) and MODIS-derived SST are presented at Fig. 3. The model shows that  
313 maximum upwelling development occurs on May 14 when the upwelling front reaches the  
314 center of the GOF and characterized by maximum temperature difference across the front  
315 up to 5°C. Unfortunately, due to heavy cloudiness, the satellite images captured only  
316 relaxation phase of the upwelling dated on May 20th.

317 As seen, the model performs better if the GLS scheme is used and the value of  $C_{lim}$   
318 is 0.53 (Galperin's value). The stronger length scale limitation leads to underestimation of  
319 mixing and increased SST values compared to MODIS data. On the other hand, the  
320 solution obtained with TKE scheme underestimates mixing, nevertheless it is not too far  
321 from the observations. The best performance takes place at the higher resolution and GLS  
322 scheme used when the solution is in a good agreement with the MODIS SST (Fig. 3b).  
323 Based on presented sensitivity tests, the GLS mixing scheme was chosen and the length  
324 scale limiting was fixed as  $C_{lim}=0.53$

325

### 326 **3.2 General model performance**

327 To evaluate the general model performance, we used in situ data for temperature  
328 and salinity obtained during Russian State Hydrometeorological University expedition  
329 dated from July 20 2011 to August 05 2011. The comparison of model and data has been  
330 performed for the last decade of July just before the UML starts to degrade due to heating  
331 and wind conditions (Fig.4). CTD data were grouped into three sets of profiles  
332 representing western (Lon 23:26, 10 profiles), central (Lon 26:28.2, 12 profiles) and  
333 eastern (Lon 28.2:30, 12 profiles) parts of the GOF. According to the presented at Fig. 4  
334 averaged CTD profiles (black curves), the UML is much deeper in the western part of the  
335 GOF and considerably shallower and sharper in the central and eastern parts. This UML  
336 behavior typical for the GOF captured quite well by all the model realizations (colored  
337 curves). Standard deviation of CTD data given as error bars presents the variability range  
338 of in situ data. All presented solutions with different parameterizations are in good  
339 agreement with the data in terms of the UML depth while the fine spatial resolution slightly  
340 better represents the nature in the western part of GOF. In the eastern part of GOF  
341 strongly influenced by the Neva outflow the modeled thermocline is about 5 m deeper than  
342 observed. This is mainly due to prescribing climatic boundary conditions at the river mouth

343 not allowing for the differences in individual years and complicated hydrodynamics of the  
344 estuary.

345 One more comparison between model and data is presented in Fig. 5 where the  
346 modeled SST for the two resolutions is given versus MODIS SST on August 2, 2011. At  
347 this time it was possible to fix the upwelling again near the southern coast of GOF. In the  
348 high resolution model solution the temperature of cold water rising to the surface drops  
349 down to 6°C that is consistent with the satellite SST. In the case of coarse resolution the  
350 upwelling effect is less pronounced: the lowest temperature in the core region is about  
351 10°C. Solutions with both resolutions reproduce spatial patterns of upwelling. Although the  
352 coarse resolution solution gives more flattened upwelling front (shown by the isotherm of  
353 19.5°C), high resolution solution is more rugged due to reproduced submesoscale features  
354 that corresponds well with observed SST.

355 Results of model comparison with SST and in situ data confirm the robustness of  
356 the developed model, which allows us to use it in a more detailed evaluation of the vertical  
357 structure formation mechanisms of the sea and its temporal evolution.

358

#### 359 **4. Results**

360 During the upwelling/downwelling event in May model on both grids simulates a  
361 substantial re-stratification of the UML. The re-stratification is characterized by sharpening  
362 and at the same time deepening of the thermocline down to 40 m near the Finnish coast  
363 and export of the cold water to the surface near the Estonian coast (Fig. 6). Fig. 6 a and b  
364 show maps of the turbocline depth on the 16th May 2011. The turbocline depth is defined  
365 as the depth at which the vertical eddy diffusivity coefficient falls below a given value (here  
366 taken equal to background value of  $5 \text{ cm}^2\text{s}^{-1}$ ) and can be interpreted as a maximum  
367 penetration depth of the turbulent motion in the surface layer.

368 According to Fig. 6a and b presenting solutions on 2 and 0.5 km grids respectively,  
369 the turbocline depth reaches the maximum in the areas near the Finnish coast where the  
370 convection is a dominant factor in vertical mixing. We can note the significant differences  
371 in the spatial patterns of the turbocline for fine and rough resolutions. Solution on 0.5 km  
372 grid shows deeper and more complex thermocline pattern. It can be explained by the fact  
373 that small-scale frontal structures induced by strong horizontal gradients and captured by  
374 the fine-resolution model lead to convective instabilities (Boccaletti et al., 2007) acting to  
375 locally restratify UML. The model with 2 km resolution cannot resolve submesoscale  
376 frontal features and high values (compare to fine resolution) of lateral diffusion coefficients  
377 act to smooth the front in other words decreasing potential energy of the front.

378 Unfortunately, few data is available for validation of these differences. Locations of CTD  
379 profiles on May 16 are marked as points I, II, III in Fig. 6a and c. Figure 6 (I, II, III) shows  
380 the vertical profiles of temperature at locations near the Finish coast. At the panel (I) the  
381 UML depth for the 2 km-resolution model (dashed black line) is shallower than the  
382 observed UML depth (solid black line) by 13 m. At the same time, observations and 0.5  
383 km-resolution model (grey line) temperature are almost collocated, and UML depth  
384 reaches 40 m. At the panel (II) modeled UML depth is overestimated, but the misfit  
385 reaches 7 m for 2 km-resolution model and only 3 m – for 0.5 km-resolution model.

386 We cannot compare the UML depth from the results presented at panel III since  
387 none of the models were able to reproduce lateral intrusions observed. The low model  
388 performance at this point can be explained by the proximity of the frontal zone between  
389 coastal and deep water masses due to the upwelling. We assume that small error in  
390 predicted location of the front can lead to serious misfits in vertical profile. Note also that  
391 the point (III) is located in a zone of rapid turbocline depth variations (see Fig. 6a and b).  
392 This fact confirms a complex front structure which is formed by the set of randomly spaced  
393 small-scale features. The deterministic model can only predict their appearance but not the  
394 exact location.

395 Figure 7 presents evolution of the thermocline through the season. Left panels  
396 present the maximum depth of the turbolcline and thermocline for the May when the  
397 thermocline was formed. Right panels present the same but for the period from 01 of Jun  
398 to 28 July. This period ends just before the upwelling in July-August from which the UML  
399 erosion begins. Thermocline depth was defined as the depth of 3.5°C isotherm (see Fig.  
400 4). As it comes from the presented data, turbulent mixing during the upwelling in May was  
401 the strongest throughout the season (see Fig.7b). At the same time increasing of the 3.5°C  
402 isotherm depth up to 45 m during June-July is not accomplished by any considerable  
403 turbulent activity (maximum turbocline depth during June-July do not exceed 20 m for the  
404 most of the area of the GOF). Taking in consideration the low value of the background  
405 vertical diffusivity coefficient ( $10^{-6} \text{ m}^2\text{s}^{-1}$ ), this fact highlights the importance of the  
406 advective processes for the formation of the shape and depth of the thermocline.  
407 Advective processes resulting in deepening of the isotherm are initiated by intrusion of  
408 warm dense water from the open boundary from the Baltic Proper. The intrusion  
409 compensates the general surface outflow from the GOF caused by rivers runoff. Notable  
410 difference in the shape of averaged profiles presented at Fig. 4 confirm this hypothesis.  
411 Eastern part of the GOF characterized by sharp and shallow thermocline and halocline.  
412 Their depths are approximately equal to the maximum turbocline depth. Turbulent and

413 heating processes are dominated here. Deepening of the thermocline and halocline down  
414 to 45 m in the western part of GOF is caused mainly by the GOF-Baltic Sea exchange  
415 processes since turbulent mixing do not penetrate at this depth here.

416 The sensitivity of the model solution to increased horizontal resolution is manifested  
417 in the different intrusion propagation to east (compare right plots on Fig. 7d and f). Density  
418 fronts associated with the intrusion are a source of baroclinic instability which are  
419 differently resolved by the 0.5 km eddy permitting configuration (Fig. 7c ) compared to 2  
420 km configuration (Fig. 7e).

421

## 422 5. Discussion and conclusions

423 We used state-of-the-art modeling framework NEMO initially developed for the open  
424 ocean to build an eddy resolving model of the GOF. To evaluate the model skill and  
425 performance two different solutions where obtained: commonly used 2 km grid and 0.5 km  
426 eddy resolving fine grid.

427 With the resolution of 0.5 km the model starts to resolve submesoscale eddies. In  
428 the ocean, submesoscales are scales of motion equal or less than the baroclinic Rossby  
429 radius of deformation. For the GOF the baroclinic Rossby radius is varying between 2-4  
430 km and we need at least 4 points to resolve the eddy. According to Gent and McWilliams  
431 (1990), the eddies can act to re-stratify the UML of the ocean, causing the vertical  
432 transport through the thermocline.

433

434 ~~In this study we were not able to identify the vertical motion in the model solution~~  
435 ~~associated with small scale eddies. The fact can be explained by the effect of~~  
436 ~~parameterization of convective processes which we cannot avoid due to hydrostatic~~  
437 ~~assumption of the model. Hydrostatic hypothesis removes convective processes from the~~  
438 ~~initial Navier-Stokes equations and so convective processes must be parameterized~~  
439 ~~instead. As it is presented in section 3.1 we had tested an interaction of all available in~~  
440 ~~NEMO parameterizations of convective processes with turbulent mixing in the frame of the~~  
441 ~~hydrostatic assumption.~~

442 By moving from 2 km to 0.5 km it is logical to expect an intensification of vertical  
443 movements induced by smaller vortices resolution. Figure 8 presents the comparison of  
444 vertical velocity absolute values for 2km and 500 m resolutions. The fields are  
445 averaged for the depth of 5 m and 5-day period in May characterized by high-intensity  
446 wind- induced dynamic. The main features of the horizontal distribution of the vertical  
447 velocity, including the regions of extreme values are similar in both cases. However, on a

448 finer grid structures resembling meanders currents and filaments appeared in the middle  
449 of the bay at the Estonian coast as well as near the Finland coast there is a set of point  
450 maxima. Both of this small scale features are absent at coarse grid. It is important to  
451 note that the difference in the vertical velocity field appear mainly in the upper mixed  
452 layer of the sea. Below the pycnocline the vertical velocity patterns in both cases are  
453 very similar. Thus, marked differences could be attributed to the vortex centers of  
454 submesoscale eddies, but this assumption is not confirmed by visual horizontal velocity  
455 field analysis: explicit vortices are absent in uv horizontal field. An alternative hypothesis  
456 links these features with local elevations of the bottom topography.  
457

458 Additional effect of resolved lateral submesoscale processes was investigated in  
459 section 4. It was shown that submesoscale motion affects the plume propagation caused  
460 by salty water intrusion to the GOF from the Baltic Sea. Generally speaking this process  
461 had found to be dominated in formation of shape of thermocline through the summer  
462 season, while the depth of UML was formed by an intensive mixing during spring  
463 upwelling. In both cases advective processes act as the main “driving force”.

464 Presented model demonstrates a substantial improvement in the basin stratification  
465 compared to previous numerical studies. Traditional point of view is that the small scale  
466 processes such as turbulence provide the majority of mixing in vertical direction. Most  
467 commonly 1-D approach is used to set up vertical mixing by tuning a turbulent scheme.  
468 For the GOF as an enclosed basin with complex bathymetry and strong stratification mixed  
469 layer dynamics can be strongly affected by lateral advective processes. Adequate  
470 representation of lateral processes by the model let us decrease the role of background  
471 constants in turbulent mixing scheme (we set them to minimum possible values). This  
472 simplifies the traditional trade-off between the depth and sharpness of the thermocline.  
473 Setting the background values of vertical eddy viscosity and diffusivity to  $10^{-5}$  and  $10^{-7}$   $\text{m}^2\text{s}^{-1}$   
474 respectively let us keep the sharp form of the thermocline and halocline while the UML  
475 depth corresponds to observations.

476 Since the time period of the runs was rather short (less than 1 year) and the model  
477 had not been used before it is obvious that the values choose of some parameters might  
478 have been somewhat improperly chosen for the use in this study. Through fine tuning of  
479 the model better results could be probably obtained. However, the focus in this study was  
480 to examine the differences arising from different horizontal resolutions, the fact that model  
481 parameters were similar in each case should be considered to be far more important than  
482 the quantitative agreement between observations and model results. Actually, it was

483 shown that the model results for both resolutions are in a reasonable agreement with  
484 available observations. In some cases 0.5 km model performs better and at the same time  
485 there are areas not covered by observations where we can note more substantial  
486 difference between models. It is found that simulations ~~which resolve~~ing submesoscale are  
487 characterized by the deeper UML with more complex structure in the regions of the GOF  
488 directly affected by the upwelling/downwelling.

489 The GOF is a highly dynamic region with lateral currenties causing the  
490 temperature contrasts and/or rapid temporal variations on the surface. From the satellite  
491 picture we can identify whether the model reproduce properly the frontal structure at the  
492 surface. For example, the temperature drop during an upwelling event and resulting  
493 temperature contrast at the surface reach 2.5 °C. We assume it to be a considerably more  
494 substantial signal comparing to known uncertainties of satellite SST measurements (0.4 °C  
495 [<https://podaac.jpl.nasa.gov>].) The usage of results of hydrodynamic modelling together  
496 with SST information can provide an extended analysis and deeper understanding of the  
497 upwelling process. Re-stratification of the UML caused by upwelling results in changes of  
498 the SST pattern that can be observed from satellites. From the comparison of modelled  
499 and observed from satellite SST we can identify whether the model reproduces the  
500 stratification itself and as a result properly reproduces the frontal structure at the surface.

501 Refinement of the model resolution below the level of 0.5 km would be of limited  
502 benefit in a hydrostatic model. For the purpose of deep investigation of submesoscale  
503 processes in GOF such as transport across the UML and on/offshore the nonhydrostatic  
504 formulation is needed. It lets us avoid "artificial smoothing" of the velocity field. Other  
505 possible improvements of the model performance, which we are planning for the next  
506 steps, will include sensitivity tests for the different boundary conditions with higher spatial  
507 resolution at the open boundary and surface and utilisation of recently available data with  
508 high spatial coverage from the expeditions during the Gulf of Finland Year 2014.

509  
510  
511  
512  
513  
514  
515  
516  
517

Отформатировано: Отступ: Первая строка: 0"

518 **Acknowledgements**

519 This work was supported by the Federal Targeted Programme for Research and  
520 Development in Priority Areas of Development of the Russian Scientific and Technological  
521 Complex for 2014-2020 (Grant Agreement No.: RFMEFI57414X0091).

522



523 **References**

- 524 Alenius, P., Myrberg, K., and Nekrasov, A.: The physical oceanography of the Gulf of  
525 Finland: a review, *Boreal Environ. Res.*, 3, 97–125, 1998.
- 526 Alenius, P., Nekrasov, A., and Myrberg, K.: The baroclinic Rossby-radius in the Gulf of  
527 Finland, *Cont. Shelf Res.*, 23, 563–573, 2003.
- 528 Andrejev, O., Sokolov, A., Soomere, T., Värvi, R., and Viikmäe, B.: The use of high-  
529 resolution bathymetry for circulation modelling in the Gulf of Finland, *Estonian Journal of*  
530 *Engineering*, 16, 187–210, 2010.
- 531 Boccaletti, G., Ferrari, R., and Fox-Kemper, B.: Mixed layer instabilities and restratification,  
532 *J. Phys. Oceanogr.*, 37, 2228–2250, 2007.
- 533 Bougeault, P. and Lacarrère, P.: Parameterization of orography-induced turbulence in a  
534 mesobeta-scale model, *Mon. Weather Rev.*, 117, 1872–1890, 1989.
- 535 Funkquist, L.: HIROMB, an operational eddy-resolving model for the Baltic Sea, *Bulletin of*  
536 *the Maritime Institute in Gdansk*, XXVIII, 7–16, 2001.
- 537 Galperin, B., Kantha, L. H., Hassid, S., and Rosati, A.: A quasi-equilibrium turbulent  
538 energy model for geophysical flows, *J. Atmos. Sci.*, 45, 55–62, 1988.
- 539 Gaspar, P., Gregoris, Y., and Lefevre, J.-M.: A simple eddy kinetic energy model for  
540 simulations of the oceanic vertical mixing: Tests at station Papa and long-term upper  
541 ocean study site, *J. Geophys. Res.*, 95, 16179–16193, 1990.
- 542 Gent, P. R. and McWilliams, J. C.: Isopycnal mixing in ocean circulation models, *J. Phys.*  
543 *Oceanogr.*, 20, 150–155, 1990.
- 544 Hankimo, J.: Some computations of the energy exchange between the sea and the  
545 atmosphere in the Baltic area, *Finnish Meteorological Office Contributions*, 57, 26 pp.,  
546 1964.
- 547 High Resolution Limited Area Modelling project HIRLAM: available at: <http://hirlam.org>, last  
548 access: 1 February 2015.
- 549 Holt, J. and Umlauf, L.: Modelling the tidal mixing fronts and seasonal stratification of the  
550 Northwest European Continental Shelf, *Cont. Shelf Res.*, 28, 887–903, 2008.
- 551 Hordoir, R., Axell, L., Loptien, U., Dietze H., and Kuznetsov, I.: Influence of sea level rise  
552 on the dynamics of salt inflows in the Baltic Sea, *J. Geophys. Res. Oceans*, 120, 6653–  
553 6668, 2015.
- 554 Hordoir, R., Dieterich, C., Basu, C., Dietze, H. and Meier, H.E.M.: Freshwater outflow of  
555 the Baltic Sea and transport in the Norwegian current: A statistical correlation analysis  
556 based on a numerical experiment, *Cont. Shelf Res.*, 64, 1–9, 2013.

557 Kantha, L. H. and Clayson, C. A.: An improved mixed layer model for geophysical  
558 applications, *J. Geophys. Res.*, 99, 25235–25266, 1994.

559 Kolmogorov, A. N.: The equation of turbulent motion in an incompressible fluid, *Izvestiya*  
560 *Akademii Nauk SSSR Seriya Fizicheskaya*, 6, 56–58, 1942.

561 Laine, A. O., Andersin, A.-B., Leinio, S., and Zuur, A. F.: Stratification-induced hypoxia as  
562 a structuring factor of macrozoobenthos in the open Gulf of Finland (Baltic Sea), *J. Sea*  
563 *Res.*, 57, 65–77, 2007.

564 Liblik, T., Lips U.: Variability of synoptic-scale quasi-stationary thermohaline stratification  
565 patterns in the Gulf of Finland in summer 2009 *Ocean Sci.*, 8, 603–614, 2012.

566 Lips, U., Lips, I., Liblik, T., and Elken, J.: Estuarine transport versus vertical movement and  
567 mixing of water masses in the Gulf of Finland (Baltic Sea), in: *US/EU-Baltic International*  
568 *Symposium, 2008 IEEE/OES*, 1–8, doi:10.1109/BALTIC.2008.4625535, Tallinn, 27–29 May  
569 2008.

570 Lips, U., Lips, I., Liblik, T., and Kuvaldina, N.: Processes responsible for the formation and  
571 maintenance of sub-surface chlorophyll maxima in the Gulf of Finland, *Estuar. Coast Shelf*  
572 *S.*, 88, 339–349, 2010.

573 Liu, H. and Holt, J. T.: Combination of the Vertical PPM Advection Scheme with the  
574 Existing Horizontal Advection Schemes in NEMO, *MyOcean Science Days*, available at:  
575 [http://mercator-](http://mercator-myocanv2.netaktiv.com/MSD2010/Abstract/AbstractLIUhedongMSD2010.doc)  
576 [myocanv2.netaktiv.com/MSD2010/Abstract/AbstractLIUhedongMSD2010.doc](http://mercator-myocanv2.netaktiv.com/MSD2010/Abstract/AbstractLIUhedongMSD2010.doc) (last  
577 access: 1 June 2013), 2010.

578 Lorke, A., Peeters, F., and Wuëst, A.: Shear-induced convective mixing in bottom  
579 boundary layers on slopes, *Limnol. Oceanogr.*, 50, 1612–1619, 2005.

580 Madec, G.: NEMO ocean engine. Note du Pôle de modélisation, Institut Pierre-Simon  
581 Laplace (IPSL), Paris, France, No 27 ISSN No 1288–1619, 2012.

582 Madec, G., Delecluse, P., Imbard, M., and Levy, C.: OPA 8.1 Ocean General Circulation  
583 Model reference manual. Note du Pole de modelisation, Institut Pierre-Simon Laplace  
584 (IPSL), Paris, France, No 11, 91 p., 1998.

585 Maximov, A. A.: Causes of the bottom hypoxia in the eastern part of the Gulf of Finland in  
586 the Baltic Sea, *Oceanology*, 46, 204–210, 2006.

587 MODIS SST: available at: <https://podaac.jpl.nasa.gov>, last access: 1 February 2015.

588 Mellor, G. L. and Yamada, T.: A hierarchy of turbulence closure models for planetary  
589 boundary layers, *J. Atmos. Sci.*, 31, 1791–1806, 1974.

590 Myrberg, K., Ryabchenko, V., Isaev, A., Vankevich, R., Andrejev, O., Bendtsen, J.,  
591 Erichsen, A., Funkquist, L., Inkala, A., Neelov, I., Rasmus, K., Medina, M. R., Raudsepp,

592 U., Passenko, J., Soderkvist, J., Sokolov, A., Kuosa, H., Anderson, T. R., Lehmann, A.,  
593 and Skogen, M. D.: Validation of three-dimensional hydrodynamic models of the Gulf of  
594 Finland, *Boreal Environ. Res.*, 15, 453–479, 2010.

595 Nekrasov, A. V. and Lebedeva, I. K.: Estimation of baroclinic Rossby radius Koporye  
596 region, *BFU Research Bulletin*, 4–5, 89–93, 2002.

597 Rantajarvi, E., Gran, V., Hällfors, S., and Olsonen, R.: Effects of environmental factors on  
598 the phytoplankton community in the Gulf of Finland – unattended high frequency  
599 measurements and multivariate analyses, *Hydrobiologia*, 363, 127–139, 1998.

600 Rippeth, T. P., Fisher, N. R., and Simpson, J. H.: The cycle of turbulent dissipation in the  
601 presence of tidal straining, *J. Phys. Oceanogr.*, 31, 2458–2471, 2001.

602 Rodi, W.: Examples of calculation methods for flow and mixing in stratified Fluids, *J.*  
603 *Geophys. Res.*, 92, 5305–5328, 1987.

604 Sokolov, A.: Modelling of submesoscale dynamics in the Gulf of Finland (Baltic Sea),  
605 *Geophysical Research Abstracts Vol. 15, EGU2013–9646*, General Assembly, Vienna,  
606 Austria, 2013.

607 Soomere, T., Myrberg, K., Leppäranta M., and Nekrasov, A.: The progress in knowledge of  
608 physical oceanography of the Gulf of Finland: a review for 1997–2007, *Oceanologia*, 50,  
609 287–362, 2008.

610 Soomere, T., Leppäranta M., and Myrberg, K.: Highlights of the physical oceanography of  
611 the Gulf of Finland reflecting potential climate changes, *Boreal Environ. Res.*, 14, 152–  
612 165, 2009.

613 Stalnacke, P., Grimvall, A., Sundblad, K., and Tonderski, A.: Estimation of riverine loads of  
614 nitrogen and phosphorus to the Baltic Sea 1970–1993, *Environ. Monit. Assess.*, 58, 173–  
615 200, 1999.

616 Stepputtis, D., Hinrichsen, H.-H., Bottcher, U., Gotze, E., and Mohrholz, V.: An example of  
617 meso-scale hydrographic features in the central Baltic Sea and their influence on the  
618 distribution and vertical migration of sprat, *Sprattus sprattus balticus* (Schn.), *Fish.*  
619 *Oceanogr.*, 20, 82–88, 2011.

620 Thomas, L., Tandon, A., and Mahadevan, A.: Submesoscale ocean processes and  
621 dynamics, in: *Ocean Modeling in an Eddy Regime*, edited by: Hecht, M. and Hasume,  
622 H., *Geophysical Monograph 177*, American Geophysical Union, Washington DC, 217–228,  
623 2007.

624 Tuomi, L., Myrberg, K., and Lehmann, A.: The performance of different vertical turbulence  
625 parameterizations in modelling the development of the seasonal thermocline in the Gulf of

626 Finland, Geophysical Research Abstracts Vol. 15, EGU2013-8229, General Assembly,  
627 Vienna, Austria, 2013.

628 Umlauf, L.: Modelling the effects of horizontal and vertical shear in stratified turbulent  
629 flows, Deep-Sea Res. Pt. II, 52, 1181–201, 2005.

630 Umlauf, L. and Burchard, H.: A generic length-scale equation for geophysical turbulence  
631 models, J. Marine Syst., 61, 235–265, 2003.

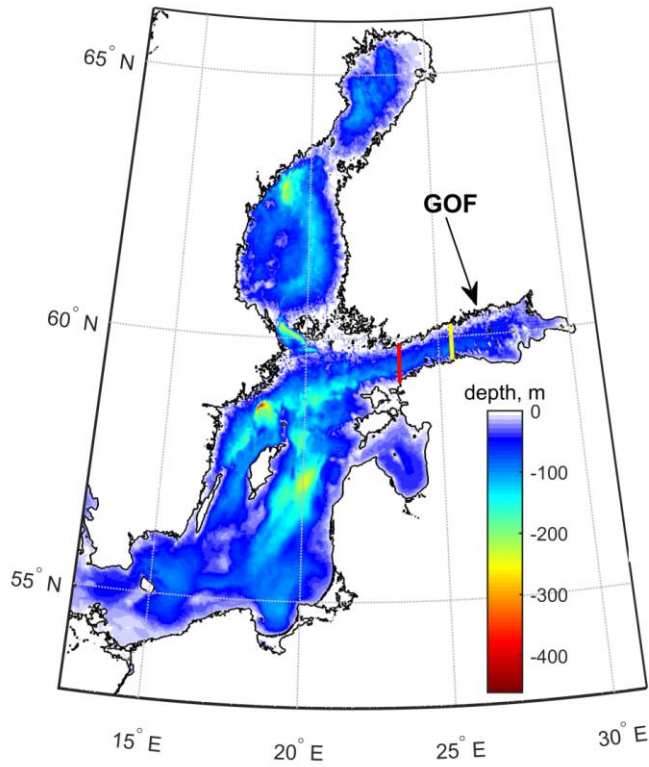
632 Umlauf, L. and Burchard, H.: Second-order turbulence closure models for geophysical  
633 boundary layers, a review of recent work, Cont. Shelf Res., 25, 795–827, 2005.

634

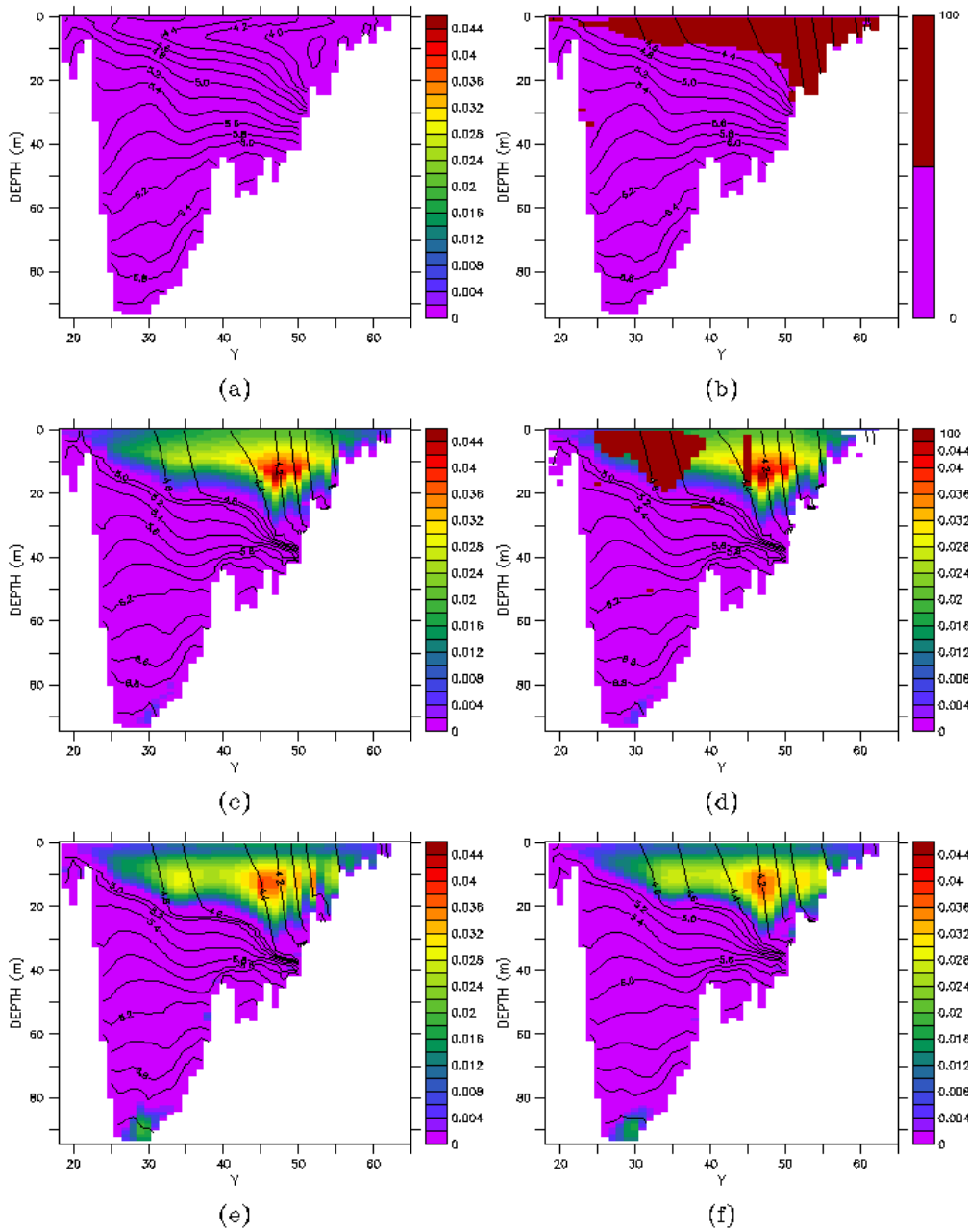
635 Zhurbas, V., Laanemets, J., and Vahtera, E.: Modeling of the mesoscale structure of  
636 coupled upwelling/downwelling events and the related input of nutrients to the upper mixed  
637 layer in the Gulf of Finland, Baltic Sea, J. Geophys. Res., 113, C05004,  
638 doi:10.1029/2007JC004280, 2008.

639

Отформатировано: английский(США)

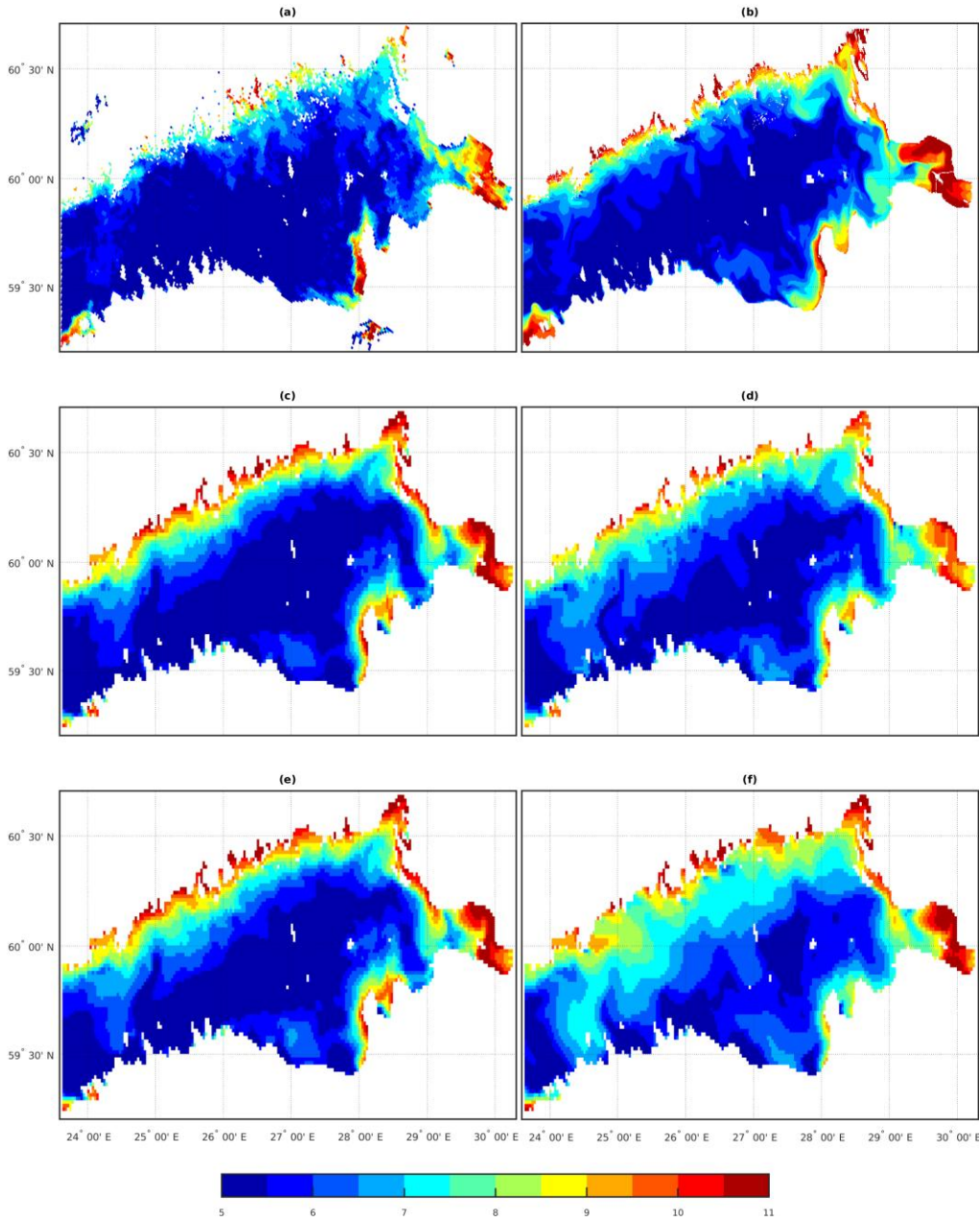


640  
641 Figure 1. The bathymetry of the Baltic Sea.  
642 Red line – open boundary of the model domain, yellow line – location of the meridional  
643 cross section for Fig. 2.



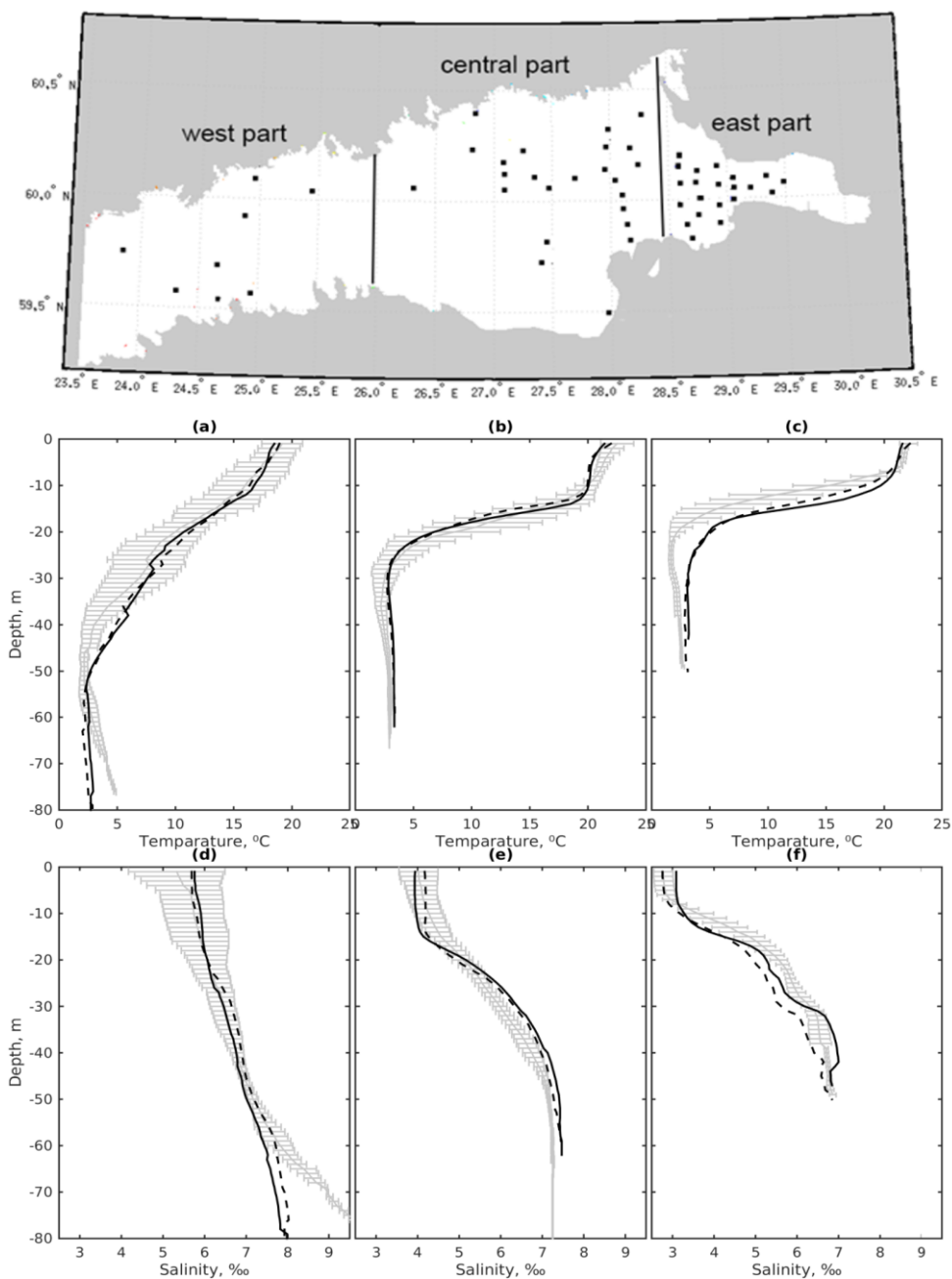
644

645 Figure 2. Meridional cross section of the GOF at 25.5°E. Vertical eddy diffusivity coefficient  
 646 (shaded surface) overlaid by density isolines: (a) constant vertical eddy viscosity/diffusivity  
 647 coefficients set to the  $10^{-4}/10^{-5} \text{ m}^2\text{s}^{-1}$ , (b) convective adjustment only (ED), (c) TKE, d) TKE  
 648 + ED, (e) GLS with Galperin limit set to 0.53, (f) GLS with Galperin limit set to 0.26.



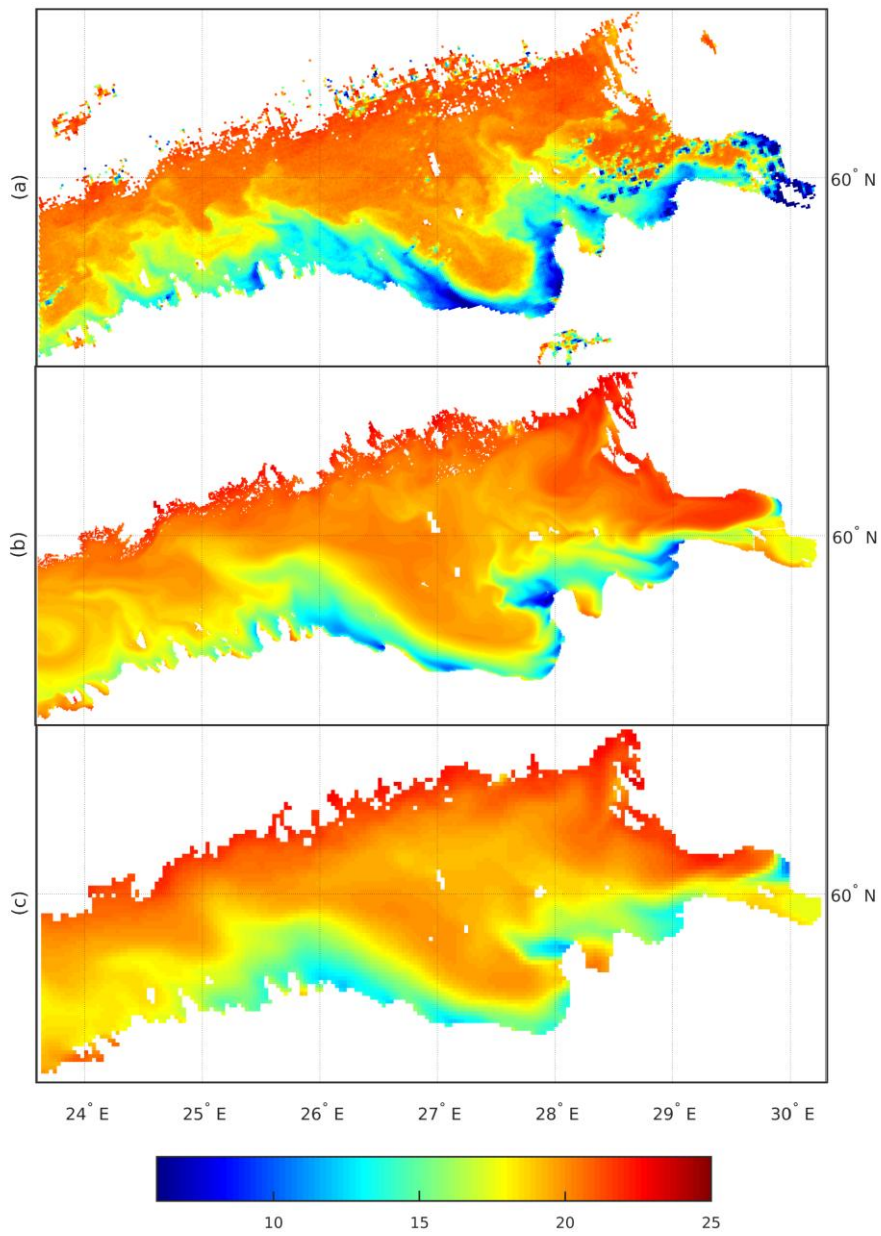
649

650 Figure3. SST on 20 May 2011: (a) MODIS SST, (b) GLS with Galperin limit 0.53 and  
 651 horizontal resolution 0.5 km, (c) GLS with Galperin limit 0.53 and horizontal resolution 2  
 652 km, (d) GLS with Galperin limit 0.26 and horizontal resolution 2 km, (e) TKE with  
 653 convective adjustment and horizontal resolution 2 km, (f) GLS with Galperin limit 0.07 and  
 654 horizontal resolution 2 km



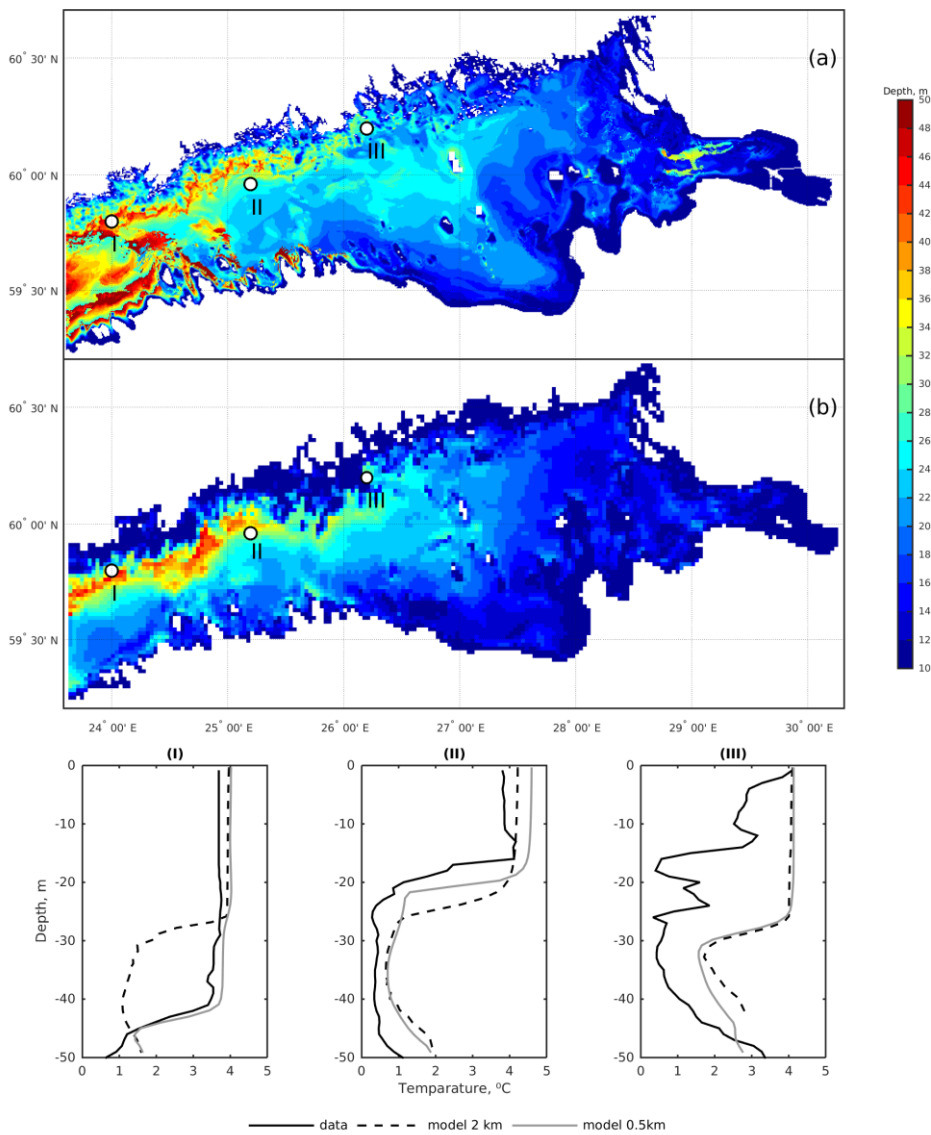
655  
 656 Figure 4. Averaged vertical profiles of temperature and salinity in West (a,d), Central (b,e)  
 657 and East (c,f) parts of GOF for the period 20 Jul – 5 Aug 2011. Grey lines – CTD data with  
 658 standard deviation corridors, solid and dashed black lines – model on grids 0.5 and 2 km  
 659 correspondently.





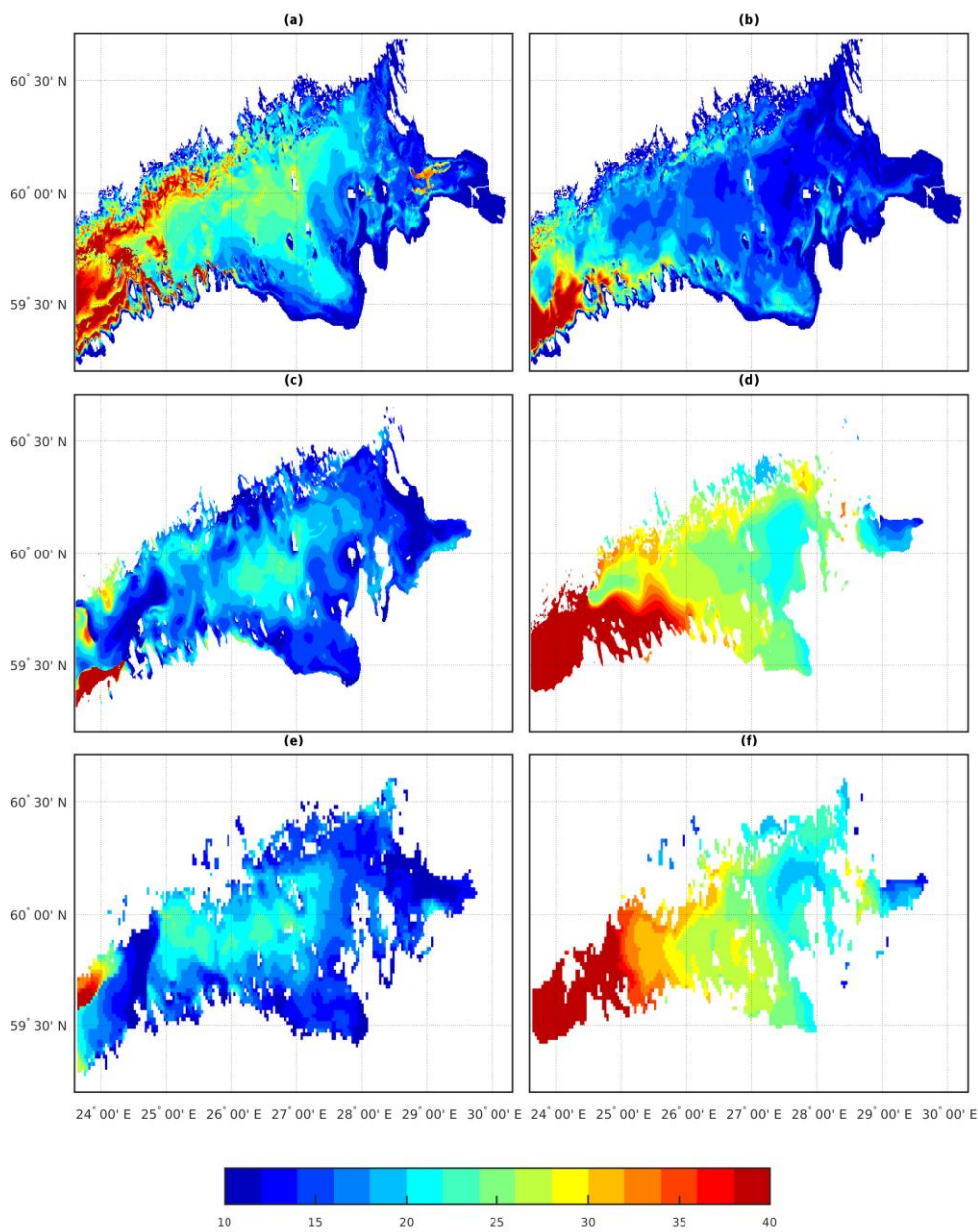
660

661 Figure 5. SST maps of GOF on 2 Aug 2011: (a) MODIS data, (b) and (c) modeled SST on  
 662 grids 0.5 and 2 km correspondently.



663

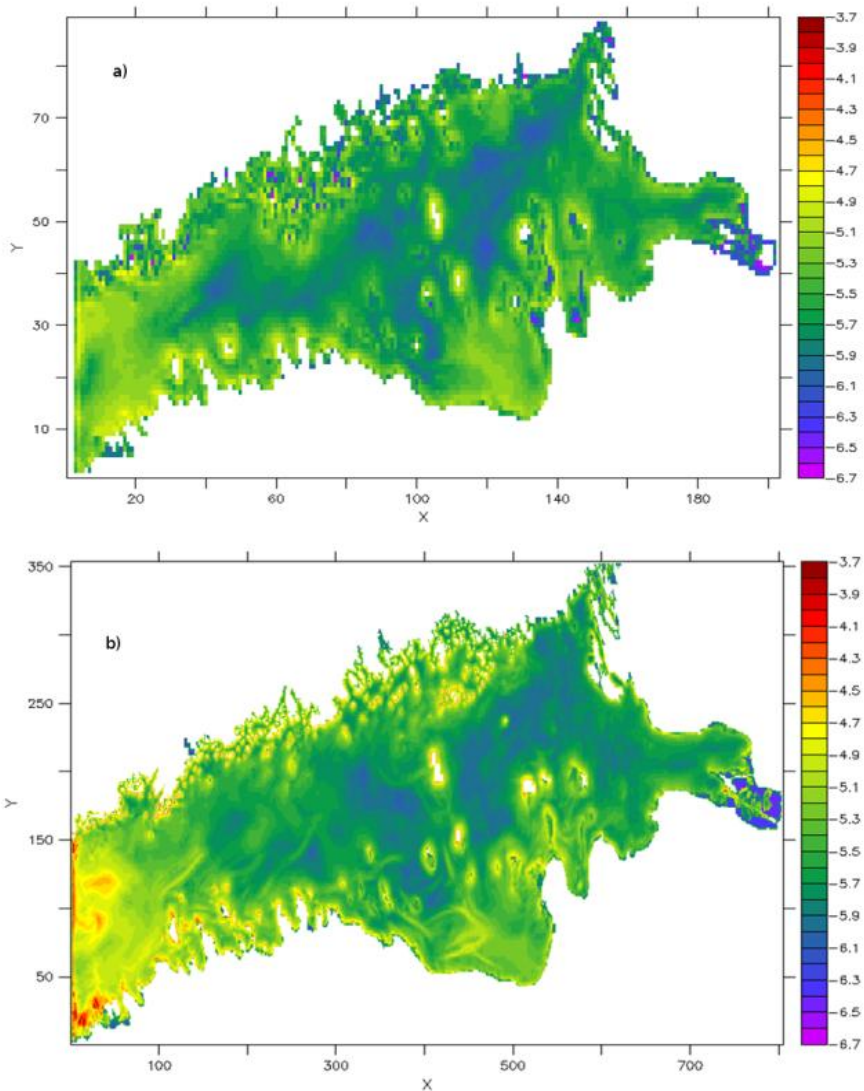
664 Figure 6. Modelled turbocline depth (m) in GOF on 20 May 2011: (a) and (b) horizontal  
 665 distributions on grids 0.5 and 2 km correspondently; (I), (II) and (III) – vertical profiles of  
 666 temperature at the locations marked on maps (a) and (b).



667

668 Figure 7. Depth of isotherm 3.5°C and turbocline depth for the periods: Left column 11-30  
 669 May 2011, Right column 1 June -28 July 2011. (a, b) – maximum turbocline depth, model  
 670 0.5 km resolution, (c, d) – isotherm 3.5°C depth model 0.5 km; (e, f) – isotherm 3.5°C  
 671 depth model 2 km.

672



Отформатировано: Шрифт: (по умолчанию)  
Times New Roman, 12 пт

Отформатировано: Междустр.интервал:  
множитель 1,15 ин

673

674

675

Figure 8 Vertical velocity absolute values (log scale) averaged for the depth of 5 m and 5-day interval: a) 2 km model grid. b) 500 m model grid